

Quantitative study of the hardening in the Alpha Magnetic Spectrometer nuclei spectra at a few hundred GV

JIA-SHU NIU (牛家树)^{1,2} AND JING LIU¹

¹*Institute of Theoretical Physics, Shanxi University, Taiyuan 030006, China*

²*State Key Laboratory of Quantum Optics and Quantum Optics Devices, Shanxi University, Taiyuan 030006, China*

ABSTRACT

The most significant feature in the cosmic-ray (CR) nuclei spectra is the spectral hardening at a few hundred GV. It is important to know whether the hardening of different nuclei species is the same or not for constructing CR sources and propagation models. In this work, we collect the recently released AMS-02 CR nuclei spectra of primary species (proton, helium, carbon, oxygen, neon, magnesium, silicon, and iron), secondary species (lithium, beryllium, boron, and fluorine), and hybrid species (nitrogen, sodium, and aluminum) and study the break positions and the spectral index differences (less and greater than the break rigidity) of the spectral hardening quantitatively. The results show us that the CR nuclei spectral hardening at a few hundred GV has hybrid origins. In detail, the dominating factors of the spectral hardening for primary and secondary CR nuclei species are different: the former comes from the superposition of different kinds of CR sources, while the latter comes from the propagation process. Both of these factors influence all kinds of CR nuclei spectra, just with different weights.

1. INTRODUCTION

The space station experiment Alpha Magnetic Spectrometer (AMS-02) improves the measurement precision of the cosmic-ray (CR) fluxes by an order of the systematics (Aguilar et al. 2013) and deepens our understanding of CRs. Based on the precision data observed by these excellent experiments represented by AMS-02, CR physics has entered a precision-driven era. More and more fine structures have been observed in CR spectra.

Up to now, AMS-02 has released all the spectra of nuclei species up to the atomic number 14 (silicon) based on its first seven years observation, including the primary CR species: proton, helium (He), carbon (C), oxygen (O), neon (Ne), magnesium (Mg), and silicon (Si) (Aguilar et al. 2021, 2020); the secondary CR species: lithium (Li), beryllium (Be), boron (B), and fluorine (F) (Aguilar et al. 2021; Aguilar et al. 2021a); the hybrid CR species: nitrogen (N), sodium (Na), and aluminum (Al) (Aguilar et al. 2018, 2021b). In addition, the spectrum of heavy primary species iron (Fe) also has been released (Aguilar et al. 2021c).

From an overall perspective, the downward trends of the secondary CR species are more serious than the primary ones, and the hybrid ones are in the middle of both. This corresponds to the origin of the secondary CR nuclei species which are produced in collisions of primary CR particles with the interstellar medium (ISM). Most of these CR nuclei species show spectral hardening at a few hundred GV, which is the most significant feature in AMS-02 nuclei spectra. The degrees of the hardening for different CR nuclei species reflect directly to the origin of the hardening, and then point to the features of CR source and propagation (Niu 2021). With the accumulation of the CR event, the uncertainties in the spectra (especially in high rigidity regions) becomes smaller and smaller. It is both necessary and possible to carry out quantitative studies on these CR nuclei spectra, which could provide us a global view when we go further into the research of CRs.

Physically speaking, the observed CR spectra are produced by the synthetic effects of the primary source injection spectra, the propagation process, and the solar modulation; even so, it is helpful to analyze the observed CR spectra directly which are always the starting point for building CR models. Although such kind of works have been simply performed in the AMS-02 data released papers (Aguilar et al. 2021, 2020; Aguilar et al. 2021b), they did not always use the independent break

power law formulas for different CR nuclei species (such as using one group of parameters to fit the spectral of He, C, and O, and using another group of parameters to fit Ne, Mg, and Si). It would cover the differences between the CR species in one group. As a result, an independent fittings to each of the CR nuclei species via a uniform method could not only provide us a detailed quantitative comparison between these species, but also give us a global view for guiding the improvements of current CR models.¹

In the following, we first introduce the methods in Section 2; the results are shown in Section 3; the discussions are presented in Section 4.

2. MATERIALS AND METHODS

Because the spectral hardening happens at a few hundred GV, the data points whose rigidity less than 45 GV are discarded in this work. In such case, we can avoid to handle the solar modulation and fit these CR nuclei spectra using a break power law directly. A break in 100-1000 GV is used to describe the position of the spectral hardening in each of the CR nuclei species.

The following formula is used to describe each of the AMS-02 nuclei spectra (including the primary CR species: proton, He, C, O, Ne, Mg, Si, and Fe; the secondary CR species: Li, Be, B, and F; the hybrid CR species: N, Na, Al) when the rigidity is greater than 45 GV:

$$F^i(R) = N^i \times \begin{cases} \left(\frac{R}{R_{\text{br}}^i}\right)^{\nu_1^i} & R \leq R_{\text{br}}^i \\ \left(\frac{R}{R_{\text{br}}^i}\right)^{\nu_2^i} & R > R_{\text{br}}^i \end{cases}, \quad (1)$$

where F is the flux of CR, N is the normalization constant, and ν_1 and ν_2 are the spectral indexes less and greater than the break rigidity R_{br} , and i denotes the species of nuclei. The errors used in our fitting are the quadratic sum of statistical and systematic errors.

The Markov Chain Monte Carlo (MCMC) framework is employed to determine the posterior probability distributions (PDF) and uncertainties of the spectral parameters for different CR nuclei species.²

3. RESULTS

¹ Our previous work (Niu 2021) performed a similar research based on an old data set from AMS-02, which showed large correlations of systematic errors. An updated data set will give us more reasonable and complete results.

² The PYTHON module `emcee` (Foreman-Mackey et al. 2013) is employed to perform the MCMC sampling. Some such examples can be referred to Niu & Li (2018); Niu et al. (2019); Niu (2022) and references therein.

The best-fit values and the allowed intervals from 5th percentile to 95th percentile of the parameters ν_1 , ν_2 , R_{br} , and $\Delta\nu \equiv \nu_2 - \nu_1$ are listed in Table 1, together with the reduced χ^2 of each fitting.³ The best-fit results and the corresponding residuals of the primary, the secondary, and the hybrid CR species are given in Figure 1, 2, and 3, respectively.⁴

Generally speaking, the reduced χ^2 s of all the CR nuclei species are smaller than 1.0, which indicates the success of the break power law to describe the spectra. But some too small reduced χ^2 s imply an improper treatment of the data errors. The improvement of the treatment needs additional information about the correlation matrix of systematic errors of AMS-02 data. Some detailed discussions of this topic can be found in Derome et al. (2019); Weinrich et al. (2020); Heisig et al. (2020). One should note that the reduced χ^2 s in Table 1 do not have the absolute meaning of goodness-of-fit, although they can be compared with each other.

4. DISCUSSIONS

In order to get a clear representation and comparison of the fitted parameters of the different nuclei species, the boxplots⁵ of the spectral parameters are used to show the distributions of ν_1 , ν_2 , R_{br} , and $\Delta\nu \equiv \nu_2 - \nu_1$ in Figure 4.

In the boxplots of ν_1 in Figure 4, the secondary species have smallest values, then the hybrid species, and then the primary CR species. It is obvious that the ν_1 values of proton and Fe are significantly different from that of the other primary CR species. The former are always referred to the p/He anomaly, which is generally ascribed to the particle-dependent acceleration mechanisms occurring in galactic CR sources (see for e.g. Vladimirov et al. (2012)). And many specific mechanisms are proposed to interpret this anomaly (see for e.g. Erlykin &

³ The information of the parameter N is not listed in the table, which is not important in the subsequent analysis. The PDF of $\Delta\nu \equiv \nu_2 - \nu_1$ is derived from that of ν_1 and ν_2 .

⁴ Note that in the lower panel of subfigures in Figs. 1, 2, and 3, the σ_{eff} is defined as

$$\sigma_{\text{eff}} = \frac{f_{\text{obs}} - f_{\text{cal}}}{\sqrt{\sigma_{\text{stat}}^2 + \sigma_{\text{sys}}^2}},$$

where f_{obs} and f_{cal} are the points which come from the observation and model calculation; σ_{stat} and σ_{sys} are the statistical and systematic standard deviations of the observed points.

⁵ A box plot or boxplot is a method for graphically depicting groups of numerical data through their quartiles. In our configurations, the band inside the box shows the median value of the dataset, the box shows the quartiles, and the whiskers extend to show the rest of the distribution which are edged by the 5th percentile and the 95th percentile.

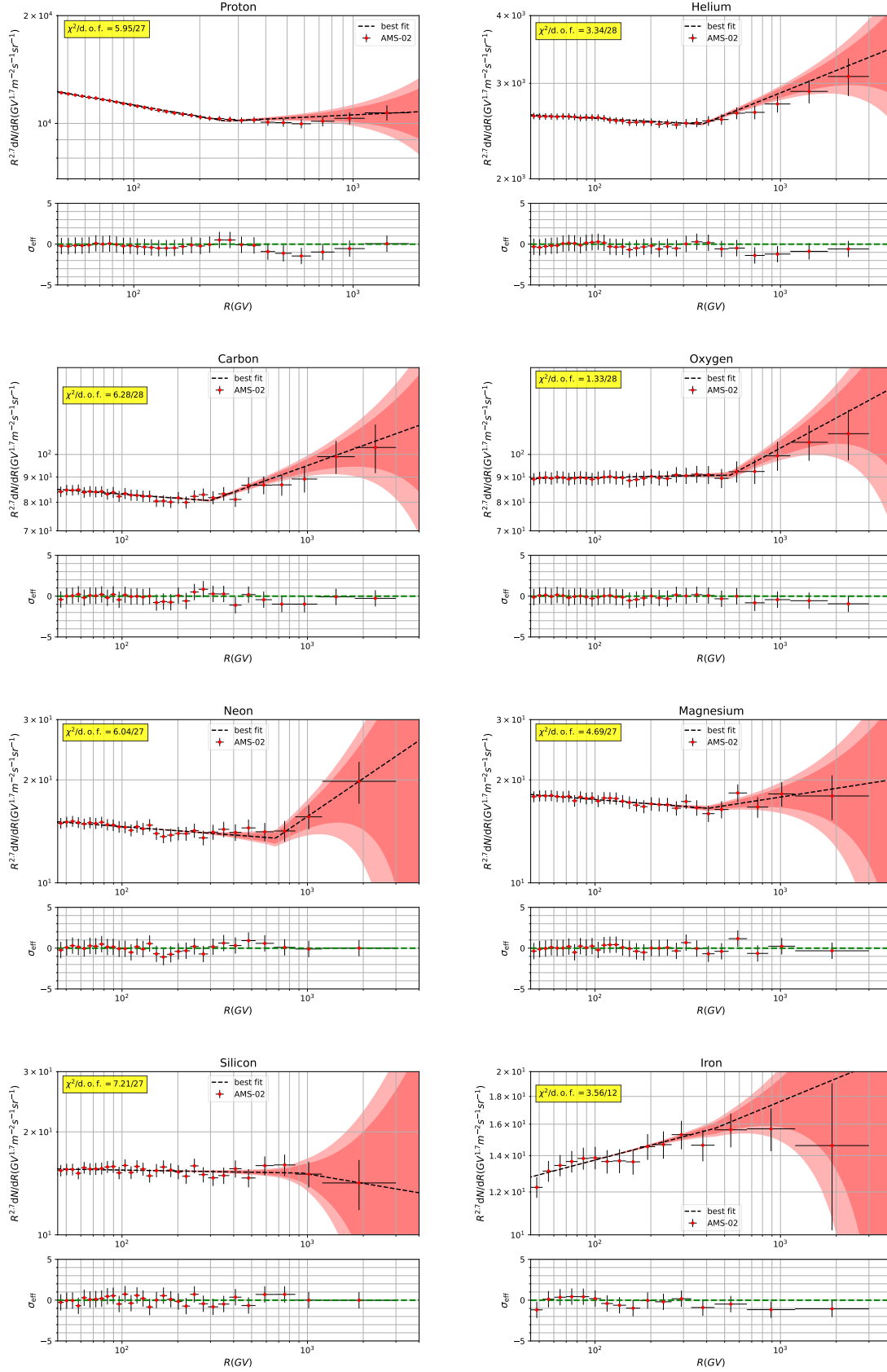


Figure 1. Fitting results and corresponding residuals to the primary CR nuclei spectra (proton, He, C, O, Ne, Mg, Si, and Fe). The 2σ (deep red) and 3σ (light red) bounds are also shown in the subfigures. The relevant reduced χ^2 of each spectrum is given in the subfigures as well.

Table 1. The fitting results of the spectral parameters for the different nuclei species. Best-fit values and allowed 5th to 95th percentile intervals (in the square brackets) are listed for each of the parameters.

| Species | ν_1 | ν_2 | R_{br} (GV) | $\Delta\nu$ | $\chi^2/\text{d.o.f}$ |
|-----------|-------------------------|-------------------------|----------------|-----------------------|-----------------------|
| proton | -2.808 [-2.814, -2.796] | -2.671 [-2.693, -2.613] | 259 [244, 348] | 0.137 [0.112,0.192] | 5.95/27 = 0.22 |
| Helium | -2.719 [-2.727, -2.709] | -2.570 [-2.602, -2.501] | 367 [318, 488] | 0.149 [0.115,0.215] | 3.34/28 = 0.12 |
| Carbon | -2.727 [-2.746, -2.707] | -2.559 [-2.619, -2.479] | 306 [217, 438] | 0.168 [0.107,0.245] | 6.28/28 = 0.22 |
| Oxygen | -2.694 [-2.709, -2.678] | -2.500 [-2.599, -2.392] | 529 [409, 676] | 0.194 [0.093,0.306] | 1.33/28 = 0.05 |
| Neon | -2.741 [-2.759, -2.719] | -2.362 [-2.568, -2.079] | 660 [542, 849] | 0.379 [0.161,0.658] | 6.04/27 = 0.22 |
| Magnesium | -2.742 [-2.765, -2.721] | -2.609 [-2.724, -2.529] | 414 [323, 464] | 0.133 [0.011,0.219] | 4.69/27 = 0.17 |
| Silicon | -2.709 [-2.729, -2.690] | -2.792 [-3.299, -2.477] | 923 [873, 994] | -0.083 [-0.585,0.230] | 7.21/27 = 0.27 |
| Iron | -2.614 [-2.647, -2.573] | -2.542 [-2.756, -2.390] | 392 [315, 544] | 0.072 [-0.171,0.239] | 3.56/12 = 0.30 |
| Lithium | -3.146 [-3.174, -3.109] | -2.836 [-2.905, -2.665] | 216 [177, 322] | 0.310 [0.239,0.470] | 17.09/27 = 0.63 |
| Beryllium | -3.102 [-3.131, -3.066] | -2.848 [-2.967, -2.657] | 247 [195, 415] | 0.254 [0.122,0.449] | 12.12/27 = 0.45 |
| Boron | -3.103 [-3.128, -3.075] | -2.765 [-2.899, -2.601] | 308 [225, 436] | 0.338 [0.201,0.492] | 7.31/27 = 0.27 |
| Fluorine | -3.016 [-3.091, -2.951] | -2.844 [-3.007, -2.712] | 189 [163, 216] | 0.172 [-0.289,0.347] | 7.55/12 = 0.63 |
| Nitrogen | -2.925 [-2.955, -2.883] | -2.694 [-2.753, -2.574] | 199 [157, 325] | 0.231 [0.158,0.335] | 15.42/27 = 0.57 |
| Sodium | -2.913 [-2.958, -2.873] | -2.657 [-3.213, -2.372] | 558 [442, 629] | 0.256 [-0.293,0.558] | 1.21/12 = 0.10 |
| Aluminum | -2.827 [-2.870, -2.785] | -2.487 [-2.733, -2.268] | 401 [270, 500] | 0.340 [0.076,0.574] | 2.71/12 = 0.23 |

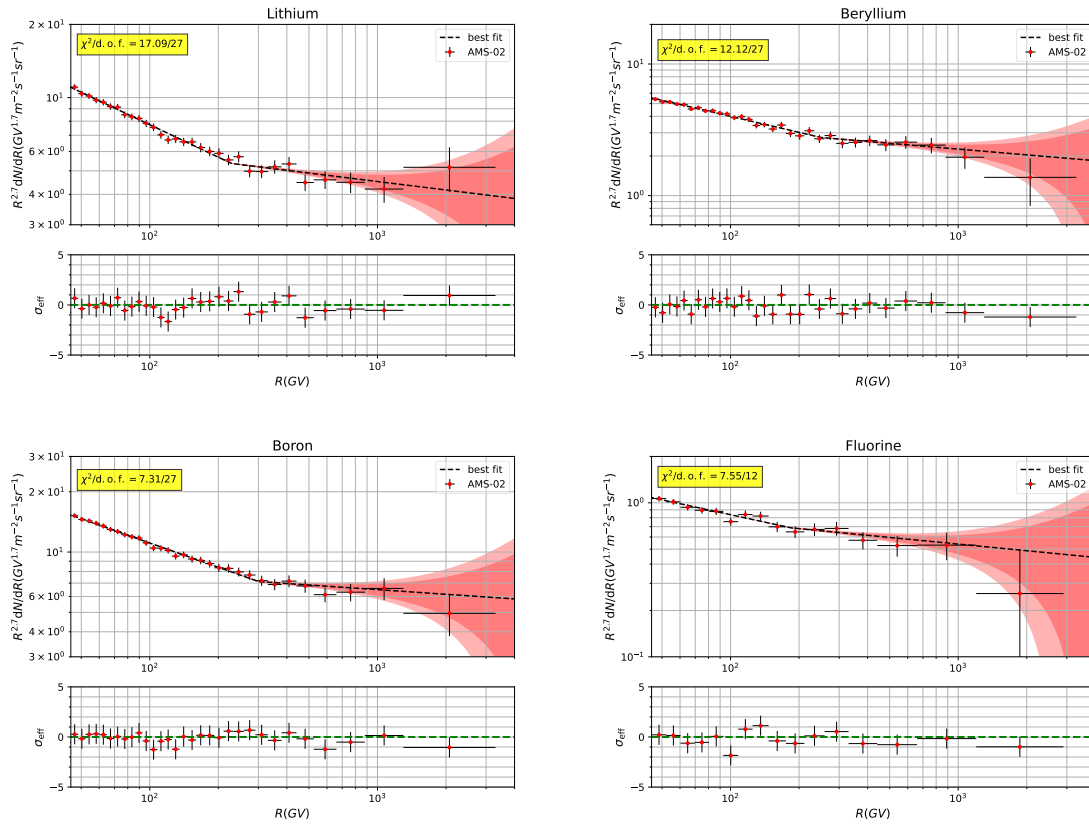


Figure 2. Fitting results and corresponding residuals to the secondary CR nuclei spectra (Li, Be, B, and F). The 2σ (deep red) and 3σ (light red) bounds are also shown in the subfigures. The relevant reduced χ^2 of each spectrum is given in the subfigures as well.

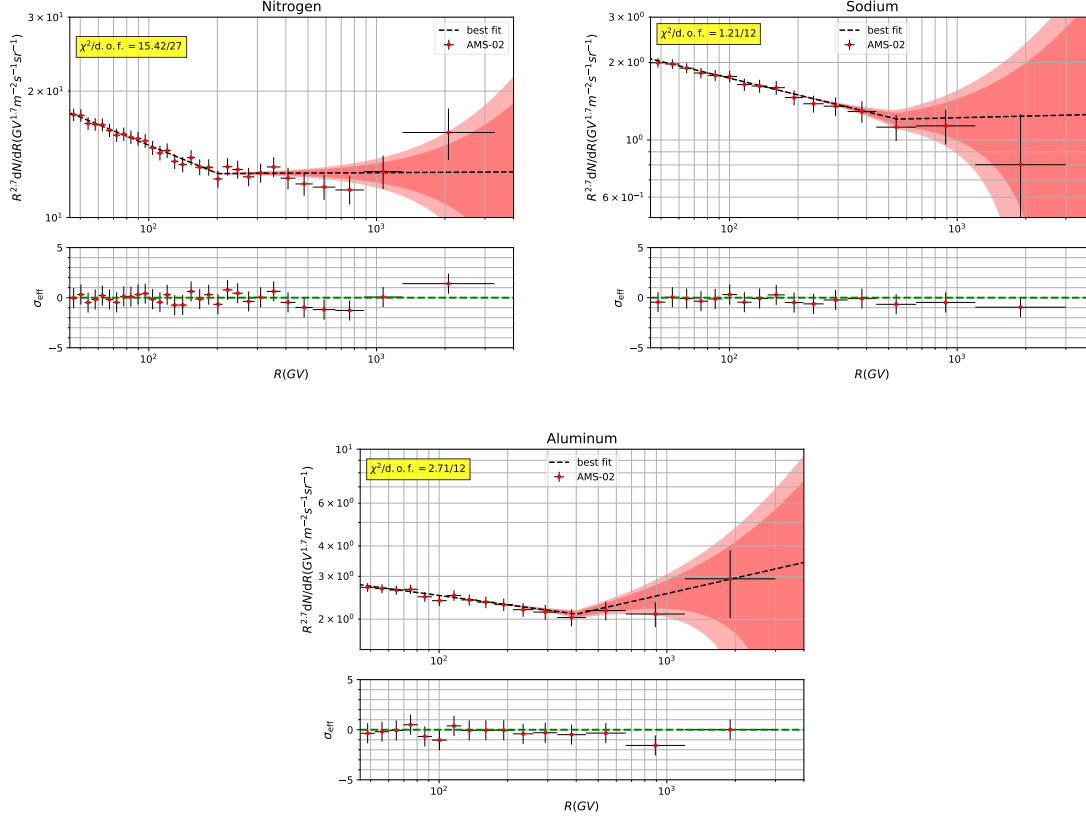


Figure 3. Fitting results and corresponding residuals to the hybrid CR nuclei spectra (N, Na, and Al). The 2σ (deep red) and 3σ (light red) bounds are also shown in the subfigures. The relevant reduced χ^2 of each spectrum is given in the subfigures as well.

Wolfendale (2015); Malkov et al. (2012); Fisk & Gloeckler (2012); Ohira & Ioka (2011); Tomassetti (2015a)). The later comes from the significantly larger interaction cross sections with the ISM of Fe than those of lighter nuclei species (He, C, O, Ne, Mg, and Si) (Aguilar et al. 2021c). For the secondary CR nuclei species, the ν_1 value of F is larger than that of others, which indicates that the propagation of heavy CRs (from F to Si) might be different from that of light CRs (from He to O). For the hybrid CR nuclei species, the ν_1 value of Al is larger than that of N and Na. This is a direct sign of its higher proportion of primary components compared with N and Na (see Aguilar et al. (2018, 2021b) for more details). One should note that a trend is implied in this subfigure: if we consider the ν_1 values in one group of CR nuclei species (primary, secondary or hybrid), they increase with the increasing of atomic number. Whether this trend is just a coincidence, or it comes from an undiscovered mechanism (such as a charge or mass dependent acceleration or propagation) should be tested in future.

In the boxplots of ν_2 in Figure 4, the uncertainties are larger than that of ν_1 because of the fewer data

points with larger uncertainties in high rigidity region. Roughly speaking, the ν_2 values of the primary CR nuclei species are larger than that of the secondary species (except that of Si with quite large uncertainty). For hybrid CR nuclei species, N has a ν_2 value with low uncertainty of about 2%, which is the same as the one for proton and within the uncertainty of the other primary species; the ν_2 uncertainty of Na is about 20%, which is similar to that of Si (about 18% - 19%); the ν_2 of Al has an uncertainty of about 9% - 10%, and is similar to the values of the primary ones, which indicates its flux in high rigidity region is dominated by the primary component.

In the boxplots of R_{br} in Figure 4, it shows that the break positions are significantly different between some of the CR nuclei species, especially in the case of primary and hybrid species. On the contrary, the break positions of the secondary CR nuclei species are distributed around 200-400 GV, which are a bit more concentrated and indicate they might have a common origin. If the spectral hardening of the secondary CR nuclei species (Li, Be, B, and F) mainly comes from their parents species (C, N, O, Ne, Na, Mg, Al, Si), their break position should

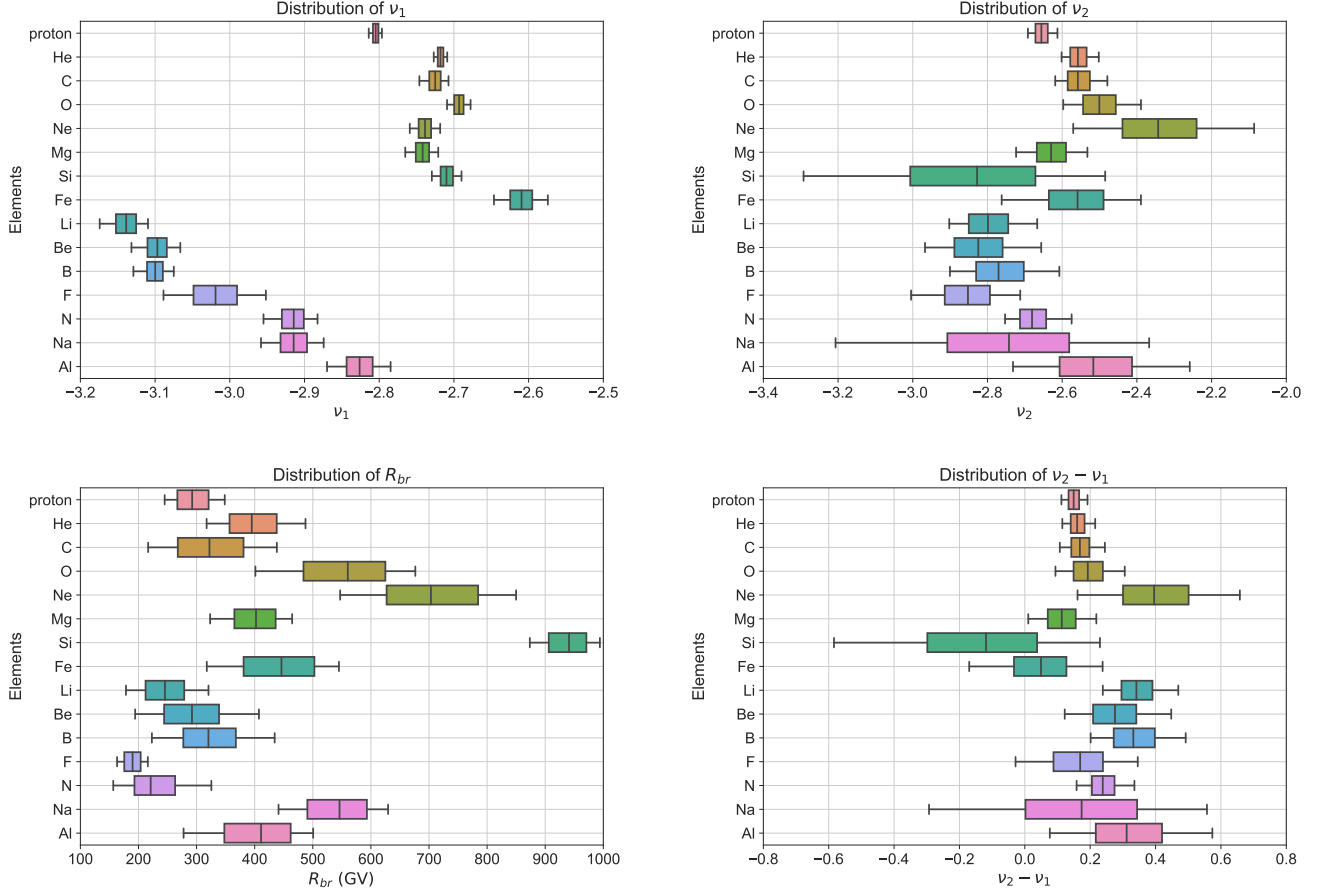


Figure 4. Boxplots for ν_1 , ν_2 , R_{br} , and $\nu_2 - \nu_1 \equiv \Delta\nu$. The band inside the box shows the median value of the dataset, the box shows the quartiles, and the whiskers extend to show the rest of the distribution which are edged by the 5th percentile and the 95th percentile.

have similar distributions. Considering the heavy secondary CR nuclei species F, it is thought to be produced mostly by the collisions of heavy nuclei (such as Ne, Mg, and Si) with the ISM, but its break position distributes around 200 GV, which is significantly different from its parents species (all of them are larger than 300 GV). This is a definite evidence that the spectral hardening in the secondary CR nuclei species does NOT dominantly inherit from its parents species, and the main factor of their hardening comes from propagation (such as in Blasi et al. (2012); Tomassetti (2012, 2015a,b); Feng et al. (2016); Génolini et al. (2017); Jin et al. (2016); Guo & Yuan (2018a,b); Liu et al. (2018); Niu et al. (2019); Boschini et al. (2020a,b); Niu (2022)). Moreover, such diffuse distributions of the break positions of the primary CR nuclei species cannot be dominantly reproduced by a uniform acceleration mechanism in CR sources or in propagation process, and the superposition of different kinds of sources (with different spectral index and element abundances) seems to be the

only natural explanation (such as in Yuan et al. (2011); Yue et al. (2019); Yuan et al. (2020); Niu (2021)).

In the boxplots of $\nu_2 - \nu_1$ in Figure 4, some of the $\Delta\nu$ values inherit large uncertainties from ν_2 , especially for Ne, Si, Fe, Na, and Al. Generally speaking, the $\nu_2 - \nu_1$ values are the same for primary, secondary, and hybrid species within the uncertainties. As the measurement of the spectral hardening, the $\Delta\nu$ of Si and Fe distribute around zero, which demonstrates the spectral hardening in these two species is not statistically significant. Moreover, it shows that the $\Delta\nu$ values of some primary CR nuclei species whose spectra have relative smaller uncertainties (proton, He, C, O, and Mg) are systematically smaller than that of the secondary species Li, Be, and B, which is the reason why some precious works claimed AMS-02 data (including the spectra or spectra ratio of Li, Be, B, C, and O) favors a break in diffusion coefficient index rather than a break in the primary source injection (see, e.g., Génolini et al. (2017); Niu & Xue (2020)). What's more interesting is that the $\Delta\nu$ of F

seems to be systematically smaller than that of Li, Be, and B. If we follow the conclusion obtained above (the spectral hardening of the secondary CR nuclei species dominately comes from the propagation process), it is an indication that the propagation properties of heavy cosmic rays, from F to Si, are different from those of light cosmic rays, from He to O (Aguilar et al. 2021a).

5. SUMMARY

In summary, for the primary CR nuclei species, although ν_1 and ν_2 have similar values within uncertainties (except the ν_1 of proton and Fe with special reasons), the significant different values of R_{br} indicate that their spectral hardening cannot come from an uniform mechanism in CR sources or propagation process. A natural origin of the hardening is the superposition of different kinds of CR sources, which in the one hand can be corresponding to the galactic averaged CR sources and a local CR source (such as Geminga SNR (Zhao et al. 2022) and the superflares from nearby M dwarfs (Ohm & Hoischen 2018)), and on the other hand can be correspond to different kinds of CR factories: such as the different population of supernova remnants (Aharonian et al. 2004), galactic center (Scherer et al. 2022), novae (H.E.S.S. Collaboration 2022), active red dwarf stars (Sinitsyna et al. 2021), etc. In both cases, as long as the CR sources have different elemental abundances, it will produce different $\nu_2 - \nu_1$ and R_{br} values for different CR nuclei species. The combination of the above two cases is also possible (Zhang et al. 2022).

For the secondary CR nuclei species, their concentrated values of R_{br} are different from that of their parents species, which denies the possibility of the inheritance from the primary species and favors the propaga-

tion origin (such as the spatial dependent propagation (Tomassetti 2012; Guo et al. 2016)). Here, the different propagation regions can be corresponding to the structures of the galaxy (i.e., the galaxy center, the bulk, the disk, the halo, and even the spiral arms), in which the densities of ISM are different and thus they have different propagation environments.

As a result, the dominating factors of the spectral hardening for primary and secondary CR nuclei species are different. Of course, these factors will influence all the CR nuclei species spectra, regardless of the primary, the secondary or the hybrid ones, just with different weights. The hybrid origins of the CR nuclei spectral hardening at a few hundred GV are also confirmed by Niu (2022) via a propagation model. This hybrid origins will not only produce a break at about 200 GV in secondary/primary ratios (such as B/C and B/O), which corresponds to the dominating spectral hardening for secondary species; but also produce breaks greater than 200 GV in secondary/primary ratios, which corresponds to the dominating spectral hardening for primary species. These predictions are confirmed by the recently released B/C and B/O ratio from DAMPE (DAMPE Collaboration 2022). Moreover, the slightly different $\Delta\nu$ and R_{br} distributions between the F and Li/Be/B show some hints that the propagation properties of heavy CRs are different from those of light CRs.

ACKNOWLEDGMENTS

Jia-Shu Niu would like to thank Hui-Fang Xue and Jue-Ran Niu for providing a quiet working environment. This research was supported by the National Natural Science Foundation of China (NSFC) (No. 12005124 and No. 12147215).

Software: `emcee` (Foreman-Mackey et al. 2013)

REFERENCES

- Aguilar, M., Alberti, G., & Alpat et al, B. 2013, Phys. Rev. Lett., 110, 141102, doi: [10.1103/PhysRevLett.110.141102](https://doi.org/10.1103/PhysRevLett.110.141102)
- Aguilar, M., Ali Cavasonza, L., & Alpat et al, B. 2018, Phys. Rev. Lett., 121, 051103, doi: [10.1103/PhysRevLett.121.051103](https://doi.org/10.1103/PhysRevLett.121.051103)
- Aguilar, M., Ali Cavasonza, L., & Ambrosi et al, G. 2020, PhRvL, 124, 211102, doi: [10.1103/PhysRevLett.124.211102](https://doi.org/10.1103/PhysRevLett.124.211102)
- Aguilar, M., Ali Cavasonza, L., Ambrosi, G., et al. 2021, PhR, 894, 1, doi: [10.1016/j.physrep.2020.09.003](https://doi.org/10.1016/j.physrep.2020.09.003)
- Aguilar, M., Cavasonza, L. A., Allen, M. S., et al. 2021a, Phys. Rev. Lett., 126, 081102, doi: [10.1103/PhysRevLett.126.081102](https://doi.org/10.1103/PhysRevLett.126.081102)
- Aguilar, M., Cavasonza, L. A., Alpat, B., et al. 2021b, Phys. Rev. Lett., 127, 021101, doi: [10.1103/PhysRevLett.127.021101](https://doi.org/10.1103/PhysRevLett.127.021101)
- Aguilar, M., Cavasonza, L. A., Allen, M. S., et al. 2021c, Phys. Rev. Lett., 126, 041104, doi: [10.1103/PhysRevLett.126.041104](https://doi.org/10.1103/PhysRevLett.126.041104)
- Aharonian, F. A., Akhperjanian, A. G., Aye, K. M., et al. 2004, Nature, 432, 75, doi: [10.1038/nature02960](https://doi.org/10.1038/nature02960)
- Blasi, P., Amato, E., & Serpico, P. D. 2012, Phys. Rev. Lett., 109, 061101, doi: [10.1103/PhysRevLett.109.061101](https://doi.org/10.1103/PhysRevLett.109.061101)
- Boschini, M. J., Della Torre, S., Gervasi, M., et al. 2020a, ApJ, 889, 167, doi: [10.3847/1538-4357/ab64f1](https://doi.org/10.3847/1538-4357/ab64f1)
- . 2020b, ApJS, 250, 27, doi: [10.3847/1538-4365/aba901](https://doi.org/10.3847/1538-4365/aba901)

- DAMPE Collaboration. 2022, *Science Bulletin*,
doi: <https://doi.org/10.1016/j.scib.2022.10.002>
- Derome, L., Maurin, D., Salati, P., et al. 2019, *A&A*, 627, A158, doi: [10.1051/0004-6361/201935717](https://doi.org/10.1051/0004-6361/201935717)
- Erlykin, A. D., & Wolfendale, A. W. 2015, *Journal of Physics G Nuclear Physics*, 42, 075201, doi: [10.1088/0954-3899/42/7/075201](https://doi.org/10.1088/0954-3899/42/7/075201)
- Feng, J., Tomassetti, N., & Oliva, A. 2016, *PhRvD*, 94, 123007, doi: [10.1103/PhysRevD.94.123007](https://doi.org/10.1103/PhysRevD.94.123007)
- Fisk, L. A., & Gloeckler, G. 2012, *ApJ*, 744, 127, doi: [10.1088/0004-637X/744/2/127](https://doi.org/10.1088/0004-637X/744/2/127)
- Foreman-Mackey, D., Hogg, D. W., Lang, D., & Goodman, J. 2013, *PASP*, 125, 306, doi: [10.1086/670067](https://doi.org/10.1086/670067)
- Génolini, Y., Serpico, P. D., & Boudaud et al, M. 2017, *Phys. Rev. Lett.*, 119, 241101, doi: [10.1103/PhysRevLett.119.241101](https://doi.org/10.1103/PhysRevLett.119.241101)
- Guo, Y.-Q., Tian, Z., & Jin, C. 2016, *ApJ*, 819, 54, doi: [10.3847/0004-637X/819/1/54](https://doi.org/10.3847/0004-637X/819/1/54)
- Guo, Y.-Q., & Yuan, Q. 2018a, *Chinese Physics C*, 42, 075103, doi: [10.1088/1674-1137/42/7/075103](https://doi.org/10.1088/1674-1137/42/7/075103)
- . 2018b, *PhRvD*, 97, 063008, doi: [10.1103/PhysRevD.97.063008](https://doi.org/10.1103/PhysRevD.97.063008)
- Heisig, J., Korsmeier, M., & Winkler, M. W. 2020, *Physical Review Research*, 2, 043017, doi: [10.1103/PhysRevResearch.2.043017](https://doi.org/10.1103/PhysRevResearch.2.043017)
- H.E.S.S. Collaboration. 2022, *Science*, 10, abn0567, doi: [10.1126/science.abn0567](https://doi.org/10.1126/science.abn0567)
- Jin, C., Guo, Y.-Q., & Hu, H.-B. 2016, *Chinese Physics C*, 40, 015101, doi: [10.1088/1674-1137/40/1/015101](https://doi.org/10.1088/1674-1137/40/1/015101)
- Liu, W., Yao, Y.-h., & Guo, Y.-Q. 2018, *ApJ*, 869, 176, doi: [10.3847/1538-4357/aaef39](https://doi.org/10.3847/1538-4357/aaef39)
- Malkov, M. A., Diamond, P. H., & Sagdeev, R. Z. 2012, *Phys. Rev. Lett.*, 108, 081104, doi: [10.1103/PhysRevLett.108.081104](https://doi.org/10.1103/PhysRevLett.108.081104)
- Niu, J.-S. 2021, *Chinese Physics C*, 45, 041004, doi: [10.1088/1674-1137/abe03d](https://doi.org/10.1088/1674-1137/abe03d)
- . 2022, *ApJ*, 932, 37, doi: [10.3847/1538-4357/ac6d5a](https://doi.org/10.3847/1538-4357/ac6d5a)
- Niu, J.-S., & Li, T. 2018, *PhRvD*, 97, 023015, doi: [10.1103/PhysRevD.97.023015](https://doi.org/10.1103/PhysRevD.97.023015)
- Niu, J.-S., Li, T., & Xue, H.-F. 2019, *ApJ*, 873, 77, doi: [10.3847/1538-4357/ab0420](https://doi.org/10.3847/1538-4357/ab0420)
- Niu, J.-S., & Xue, H.-F. 2020, *JCAP*, 2020, 036, doi: [10.1088/1475-7516/2020/01/036](https://doi.org/10.1088/1475-7516/2020/01/036)
- Ohira, Y., & Ioka, K. 2011, *ApJL*, 729, L13, doi: [10.1088/2041-8205/729/1/L13](https://doi.org/10.1088/2041-8205/729/1/L13)
- Ohm, S., & Hoischen, C. 2018, *MNRAS*, 474, 1335, doi: [10.1093/mnras/stx2806](https://doi.org/10.1093/mnras/stx2806)
- Scherer, A., Cuadra, J., & Bauer, F. E. 2022, *A&A*, 659, A105, doi: [10.1051/0004-6361/202142401](https://doi.org/10.1051/0004-6361/202142401)
- Sinitsyna, V. G., Sinitsyna, V. Y., & Stozhkov, Y. I. 2021, *Astronomische Nachrichten*, 342, 342, doi: [10.1002/asna.202113931](https://doi.org/10.1002/asna.202113931)
- Tomassetti, N. 2012, *ApJL*, 752, L13, doi: [10.1088/2041-8205/752/1/L13](https://doi.org/10.1088/2041-8205/752/1/L13)
- . 2015a, *ApJL*, 815, L1, doi: [10.1088/2041-8205/815/1/L1](https://doi.org/10.1088/2041-8205/815/1/L1)
- . 2015b, *PhRvD*, 92, 081301(R), doi: [10.1103/PhysRevD.92.081301](https://doi.org/10.1103/PhysRevD.92.081301)
- Vladimirov, A. E., Jóhannesson, G., & Moskalenko et al, I. V. 2012, *ApJ*, 752, 68, doi: [10.1088/0004-637X/752/1/68](https://doi.org/10.1088/0004-637X/752/1/68)
- Weinrich, N., Génolini, Y., Boudaud, M., Derome, L., & Maurin, D. 2020, *A&A*, 639, A131, doi: [10.1051/0004-6361/202037875](https://doi.org/10.1051/0004-6361/202037875)
- Yuan, Q., Qiao, B.-Q., Guo, Y.-Q., Fan, Y.-Z., & Bi, X.-J. 2020, *Frontiers of Physics*, 16, 24501, doi: [10.1007/s11467-020-0990-4](https://doi.org/10.1007/s11467-020-0990-4)
- Yuan, Q., Zhang, B., & Bi, X.-J. 2011, *PhRvD*, 84, 043002, doi: [10.1103/PhysRevD.84.043002](https://doi.org/10.1103/PhysRevD.84.043002)
- Yue, C., Ma, P.-X., & Yuan et al, Q. 2019, *Frontiers of Physics*, 15, 24601, doi: [10.1007/s11467-019-0946-8](https://doi.org/10.1007/s11467-019-0946-8)
- Zhang, Y., Liu, S., & Zeng, H. 2022, *MNRAS*, 511, 6218, doi: [10.1093/mnras/stac470](https://doi.org/10.1093/mnras/stac470)
- Zhao, B., Liu, W., Yuan, Q., et al. 2022, *ApJ*, 926, 41, doi: [10.3847/1538-4357/ac4416](https://doi.org/10.3847/1538-4357/ac4416)